



Dopamine Release in the Nonhuman Primate Caudate and Putamen Depends upon Site of Stimulation in the Subthalamic Nucleus

Hoon-Ki Min,^{1,2,3*} Erika K. Ross,^{1*} Hang Joon Jo,¹  Shinho Cho,¹ Megan L. Settell,¹ Ju Ho Jeong,^{1,5} Penelope S. Duffy,¹ Su-Youne Chang,^{1,2} Kevin E. Bennet,^{1,4}  Charles D. Blaha,¹ and Kendall H. Lee^{1,2}

¹Department of Neurologic Surgery, ²Department of Physiology and Biomedical Engineering, ³Department of Radiology, and ⁴Division of Engineering, Mayo Clinic, Rochester, Minnesota 55905, and ⁵Department of Neurosurgery, Dongguk University Gyeongju Hospital, Gyeongbuk 780-350, Korea

Deep brain stimulation (DBS) of the subthalamic nucleus (STN) is an effective treatment for medically refractory Parkinson's disease. Although DBS has recognized clinical utility, its biologic mechanisms are not fully understood, and whether dopamine release is a potential factor in those mechanisms is in dispute. We tested the hypothesis that STN DBS-evoked dopamine release depends on the precise location of the stimulation site in the STN and the site of recording in the caudate and putamen. We conducted DBS with miniature, scaled-to-animal size, multicontact electrodes and used functional magnetic resonance imaging to identify the best dopamine recording site in the brains of nonhuman primates (rhesus macaques), which are highly representative of human brain anatomy and circuitry. Real-time stimulation-evoked dopamine release was monitored using *in vivo* fast-scan cyclic voltammetry. This study demonstrates that STN DBS-evoked dopamine release can be reduced or increased by redirecting STN stimulation to a slightly different site.

Key words: caudate; deep brain stimulation; dopamine; fast-scan cyclic voltammetry; functional magnetic resonance imaging; subthalamic nucleus

Significance Statement

Electrical stimulation of deep structures of the brain, or deep brain stimulation (DBS), is used to modulate pathological brain activity. However, technological limitations and incomplete understanding of the therapeutic mechanisms of DBS prevent personalization of this therapy and may contribute to less-than-optimal outcomes. We have demonstrated that DBS coincides with changes in dopamine neurotransmitter release in the basal ganglia. Here we mapped relationships between DBS and changes in neurochemical activity. Importantly, this study shows that DBS-evoked dopamine release can be reduced or increased by refocusing the DBS on a slightly different stimulation site.

Introduction

Deep brain stimulation (DBS) of the subthalamic nucleus (STN) has become an effective treatment for medically refractory Par-

kinson's disease (PD; Shen, 2014). Even though DBS is recognized for its clinical efficacy in the treatment of certain neurologic conditions, the biological mechanisms of DBS are still not fully understood. While there are unquestionably multiple complex local and circuitry effects of DBS, there is conflicting evidence about whether STN DBS evokes dopamine release. Clarity on this issue has implications for the role of DBS in triggering neurochemical changes.

Indirect evidence suggests that STN DBS has dopaminergic effects. It often reduces and sometimes eliminates the need for

Received Feb. 5, 2016; revised April 18, 2016; accepted April 20, 2016.

Author contributions: H.-K.M., S.-Y.C., K.E.B., C.D.B., and K.H.L. designed research; H.-K.M., E.K.R., M.L.S., J.H.J., and S.-Y.C. performed research; H.J.J. and K.E.B. contributed unpublished reagents/analytic tools; H.-K.M., E.K.R., H.J.J., S.C., and M.L.S. analyzed data; H.-K.M., E.K.R., H.J.J., S.C., M.L.S., P.S.D., C.D.B., and K.H.L. wrote the paper.

This work was supported by the National Institutes of Health (NIH; R01 NS 70872, to K.H.L.) and The Grainger Foundation. We thank Andrea McConico, Michael Marsh, Jill Anderson, Kip Ludwig, and Allan Bieber for their support and advices; Steve Goerss, Bruce Kall, and Seong Rok Han for their surgical support; Dong-Pyo Jang and Yoonbae Oh for their advice on electrochemistry; Kendall Dennis, Bruce Gustine, and their colleagues at the Mayo Clinic Division of Engineering for their support; Jodi Silvernail and the Mayo Clinic Department of Comparative Medicine for animal care; and Diane Sauter and the Mayo Clinic Center for Advanced Imaging Research at the Mayo Clinic for their support (NIH C06 RR018898).

*H.-K.M. and E.K.R. contributed equally to this work.

The authors declare no competing financial interests.

This article is freely available online through the *J Neurosci* Author Open Choice option.

Correspondence should be addressed to Dr. Kendall H. Lee, PhD, Mayo Clinic, 200 First Street SW, Rochester, MN 55905. E-mail: lee.kendall@mayo.edu.

DOI:10.1523/JNEUROSCI.0403-16.2016

Copyright © 2016 Min, Ross et al.

This is an Open Access article distributed under the terms of the Creative Commons Attribution License Creative Commons Attribution 4.0 International, which permits unrestricted use, distribution and reproduction in any medium provided that the original work is properly attributed.

dopaminergic medications, such as levodopa (Moro et al., 1999). Also STN DBS can elicit dyskinesias, a result similar to the adverse effects of excess levodopa (Benabid et al., 2000). In addition, the best electrode location when targeting the STN is considered to be in the area immediately dorsal to the STN (Starr et al., 2002), which, among many other neurotransmitter pathways, contains surviving fibers of the dopaminergic nigrostriatal pathway (Parent et al., 2000). Preclinical studies of STN stimulation-evoked dopaminergic transmission in both intact and dopamine-depleted animal models have found that DBS evokes dopamine release in rodents (Bruet et al., 2001; Meissner et al., 2003; Lee et al., 2006), in swine (Shon et al., 2010), and in nonhuman primates (NHPs; Gale et al., 2013).

However, four positron emission tomography (PET) studies of PD patients with STN DBS stand in contrast to these animal model findings. All four [^{11}C] raclopride (RAC) PET studies failed to demonstrate dopamine release despite improvement in PD motor symptoms by STN DBS (Abosch et al., 2003; Hilker et al., 2003; Strafella et al., 2003; Thobois et al., 2003).

It is possible that the basis for these conflicting findings is specific to methodological differences among them. Studies have shown that the occurrence and overall magnitude of dopamine transmission evoked by STN DBS is highly dependent upon the anatomic location of the stimulating electrode within the STN and its relative proximity to neighboring neural elements, as well as on the configuration of the stimulating electrode (Lozano et al., 2002; McIntyre et al., 2004). Stimulation location and its current spread may contribute as well to the inconsistencies that can occur in neurophysiological and behavioral outcomes of STN DBS (Kringelbach et al., 2007), the variability of which has not been thoroughly accounted for in previous dopamine DBS studies.

The objective of this study was to characterize STN DBS-evoked dopamine release as a function of the location of the DBS electrode within the STN and of the neurochemical recording electrode in the caudate and putamen. We conducted STN DBS with scaled-to-animal size, miniaturized, multicontact DBS electrodes in the brains of intact NHPs, which are highly representative of human brain anatomy and circuitry. Stimulation-evoked dopamine release was monitored in the caudate and putamen using real-time *in vivo* fast-scan cyclic voltammetry (FSCV), supporting subsecond time resolution, micrometer-dimension spatial resolution, and chemical selectivity (Garris et al., 1994).

Since the magnitude of dopamine release may vary within structures targeted for neurochemical recording, we also investigated a new method of determining the optimal location for recording DBS-evoked dopamine in the caudate and putamen which was guided by voxel-specific functional magnetic resonance imaging (fMRI; Min et al., 2014). Overall, we found that the magnitude of STN DBS-evoked extracellular dopamine release in the caudate and putamen was dependent upon the locus of the stimulation site in the STN and the fMRI-identified recording sites in the caudate and the putamen.

Materials and Methods

Animals. The study group consisted of intact male rhesus macaques ($n = 3$; M1–M3) weighing an average of 12 ± 1 kg. All study procedures were compliant with the National Institutes of Health Guidelines for Animal Research and approved by the Mayo Clinic Institutional Animal Care and Use Committee.

DBS surgery. Surgical procedures were performed as described by Min et al. (2014). Sedation was maintained with 1.75–2.5% isoflurane during surgery and 1.5–1.75% during the fMRI and FSCV experiments. Vital signs were monitored throughout all the procedures. An MRI-guided stereotactic targeting system, specifically developed for NHP, was used

for stimulating electrode targeting and implantation. All imaging was conducted by a 3T MRI scanner (Signa HDx, General Electric). A miniature platinum-iridium DBS electrode (NuMed), consisting of six cylindrical contacts ($625 \mu\text{m}$ in diameter and $500 \mu\text{m}$ in length, numbered ventrodorsally from c1 to c6; Fig. 1C) and separated by $500 \mu\text{m}$, was introduced unilaterally to the STN. Our DBS surgical trajectories were planned to avoid penetration of crucial cortices (motor and sensory) and nuclei (caudate, putamen, and thalamus) at an angle from the posterior border of parietal lobe to an anterior ventral passage, which would also prevent fMRI artifact in our regions of interest (Table 1). Electrode location was confirmed by x-ray fluoroscopy (Siremobil Compact, Siemens) during surgery and by three-dimensional (3-D) computed tomography (CT; Somatom Definition, Siemens) postoperatively. DBS electrode impedance was checked postsurgery and throughout the fMRI and FSCV experiments ($2000\text{--}3000 \Omega$). One of the contacts (c5, M1) showed high impedance ($>10,000 \Omega$) and was thus eliminated from any experiments. DBS electrodes were implanted for chronic stimulation, followed by 1–2 months of postsurgical recovery.

fMRI during electrical stimulation. fMRI experiments were performed during monopolar monophasic (charged balanced) stimulation pulses at 130 Hz, 3–4 V, and 150–250 μs pulse duration (Stimulator Model 3550, Medtronic). fMRI was conducted using a gradient echo (GRE) echo-planar imaging pulse sequence (integrated spatial spectral pulse for fat suppression) with an anatomical 2-D T2-weighted GRE image. An event-related-like block design was used to detect BOLD responses evoked by electrical stimulation, performing five stimulus/rest blocks (6 s ON/60 s OFF). For data processing, a standard preprocessing sequence was performed, including slice scan time correction, 3-D motion correction, and temporal filtering (BrainVoyager QX, Brain Innovation). Neither spatial smoothing nor normalization was applied. To correct for multiple comparisons and exclude false-positive voxels, we considered only voxels with a false discovery rate of <0.001 as representing sites of activation (Min et al., 2014).

FSCV. fMRI imaging results were used to determine the maximum *t*-score voxel of BOLD activation neurochemical recording target within the caudate and putamen in all three subjects (Fig. 1H,J). As described by Chang et al. (2012), voltammetric recordings were performed using FSCV with conventional carbon fiber microelectrodes (CFMs) for the actual electrochemical recording. Each electrode had an exposed diameter of $7 \mu\text{m}$ and a length of $\sim 100 \mu\text{m}$. FSCV was performed wirelessly using the Mayo Clinic-developed Wireless Instantaneous Neurotransmitter Concentration Sensor Harmoni system (Chang et al., 2013). The CFM was held at -0.4 V, and triangular waveforms (-0.4 to 1.5 V vs Ag/AgCl at 900 V/s) were applied at 10 Hz. Background-subtracted cyclic voltammogram currents were obtained by subtracting the average of 10 voltammograms obtained before electrical stimulation from each poststimulation voltammogram. For the FSCV experiments, a 2 s stimulation was followed by a 5 min rest period performed to maintain turnover time, while approaching the target using a high-precision computer-controlled microdrive to lower the electrodes in $100 \mu\text{m}$ increments (Alpha Omega). Postcalibration was conducted on the CFMs, and the voltammetry current results were normalized using gamma value (Heien et al., 2003).

DBS electrode contact localization. All imaging data were processed and analyzed by Analysis of Functional NeuroImages (AFNI). Preoperative high-resolution MRI (resolution: 0.3 mm isovoxel) and postoperative CT (resolution: 0.2 mm isovoxel) confirmed the location of the STN target and each miniaturized DBS electrode contact. As shown in Figure 1A,B, intermodal spatial registration between MRI and CT images confirmed (Lauro et al., 2016) that the DBS electrode was penetrating the STN in each subject. Each subject's MRI–CT fusion image was normalized using nonrigid morphing weighted in the midbrain to a macaque brain template (Van Essen et al., 2012), and an active contour tool (Yushkevich et al., 2006) was used to determine the boundaries of the STN and the red nucleus (RN) as projected onto a 3-D model based on the imaging data (Fig. 1D). This procedure allowed identification of each DBS contact from each subject within the 3-D model of the STN (Fig. 1E). All DBS contacts projected onto the 3-D STN model. Figure 1F shows DBS contacts in a normalized MRI–CT fusion image for all three subjects. These procedures were performed blinded to the fMRI and FSCV results (by

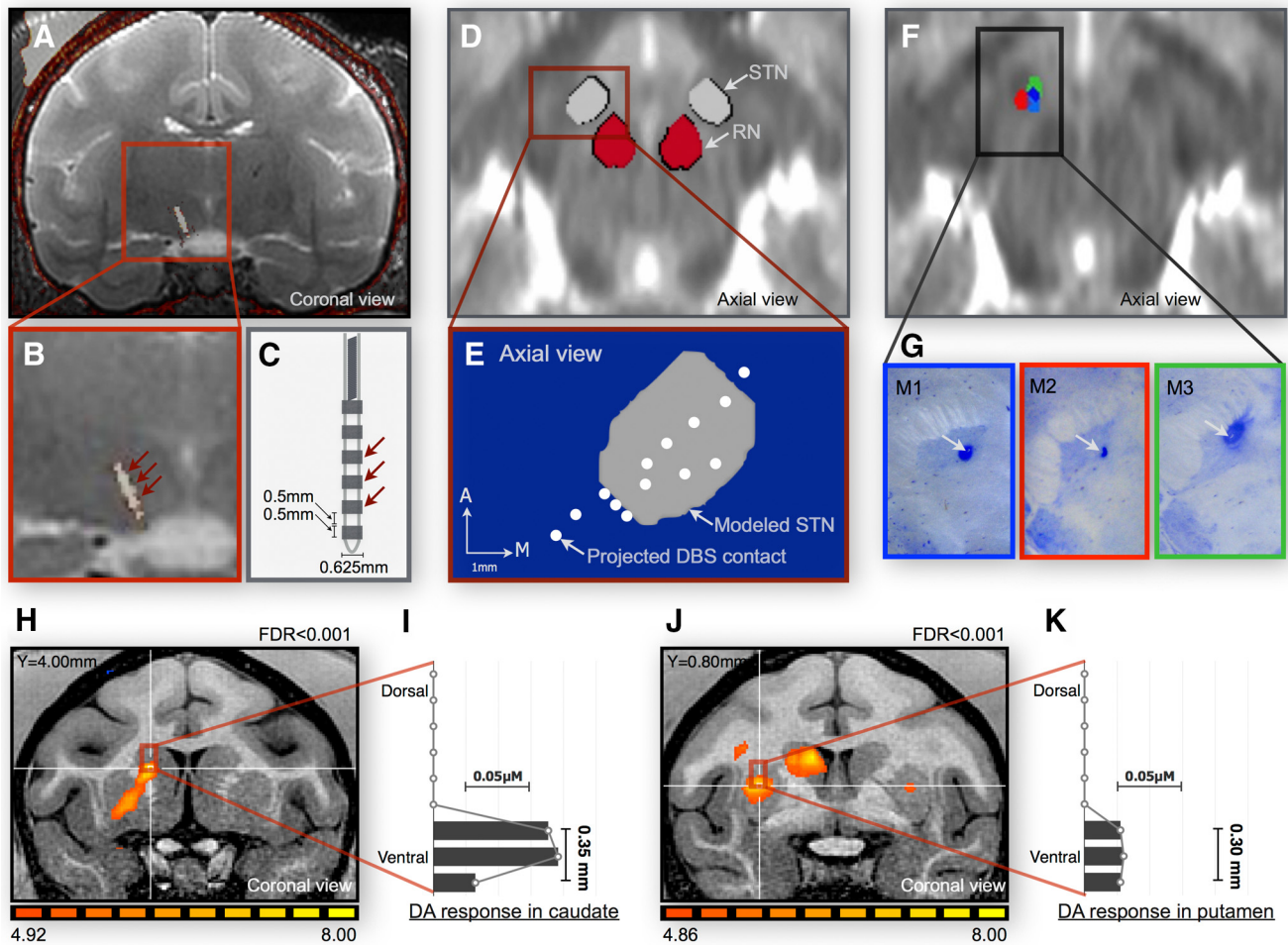


Figure 1. DBS and CFM targeting and confirmation. *A*, within-subject MRI and CT fusion results showing the precise location of each DBS contact in the STN. *B*, Expanded view of the MRI–CT fusion image in a single subject showing the DBS electrode contact locations. *C*, Schematic image of the multicontact miniature DBS electrode. *D*, cross-modality registration for each subject’s MRI–CT fusion image to an NHP brain template in which the location of STN is shown in gray and the RN in red during 3-D coregistration using a normalized averaged T2 image from each subject (axial view). *E*, Projection of all of the DBS contacts from each subject onto the 3-D STN model in a representative axial slice. *F*, DBS contacts from each subject (indicated by red, green, and blue) following normalization (axial view). *G*, DBS electrode location as confirmed by cresyl violet staining. *H, J*, fMRI confirmation of the recording location in the caudate and putamen. *I, K*, Histograms of stimulation-evoked peak dopamine responses occurring selectively within regions of the caudate and putamen identified by maximum *t*-score BOLD voxel.

Table 1. Experiment parameters for stimulation and recording targets

Subject	STN target coordinate (from midanterior and posterior commissure)	fMRI stimulation parameter	FSCV caudate target coordinate (from anterior commissure)	FSCV putamen target coordinate (from anterior commissure)	FSCV stimulation parameter
M1	(6.00 L, 0.25 A, 7.25 I, 120° collar, 61° arc)	130 Hz 4V 100 µs	(5.25 L, 3.50 A, 7.50 S)	(12.50 L, 1.25 A, 4.75 S)	130 Hz 4 V 250 µs
M2	(5.00 L, 0.00 P, 4.00 I, 120° collar, 67° arc)	130 Hz 3V 100 µs	(5.25 L, 2.00 A, 7.25 S)	(10.75 L, 2.00 P, 4.25 S)	130 Hz 3V 150 µs
M3	(5.50 R, 0.75 P, 4.00 I, 116° collar, 120° arc)	130 Hz 4V 100 µs	(4.25 R, 7.75 A, 2.50 S)	(9.00 R, 6.00 A, 0.00 S)	130 Hz 4 V 250 µs

L, Left; R, Right; A, Anterior; P, Posterior; I, Inferior; S, Superior.

H.J.J.). The DBS electrode location was further confirmed histologically by cresyl violet staining (Fig. 1G).

Estimation of the spatial relationship between STN stimulation site and evoked caudate and putamen dopamine release. We overlaid an evoked dopamine volume projection color map from the caudate and putamen on to the STN DBS contact location model using all of the DBS contact results from all the NHP subjects (total *n* = 51 data points each for caudate and putamen). The dopamine results underwent bilinear interpolation (Szeliski, 1990), generating a distribution color map, which indicated the relative peak magnitude of the evoked dopamine response. We plotted the evoked dopamine response as a function of its anatomical location distance around the STN for three orthogonal planes. The Pear-

son correlation coefficient between the directional distance for each axis and dopamine magnitude was calculated independently for the caudate and the putamen.

Results

Confirmation of recording location in the caudate and putamen

Individual DBS–fMRI studies (resolution: 2.4 mm isovoxel) were conducted to identify the best recording location within the caudate and the putamen of each subject. Consistent with previous findings, upon stimulation, areas of BOLD activation were found

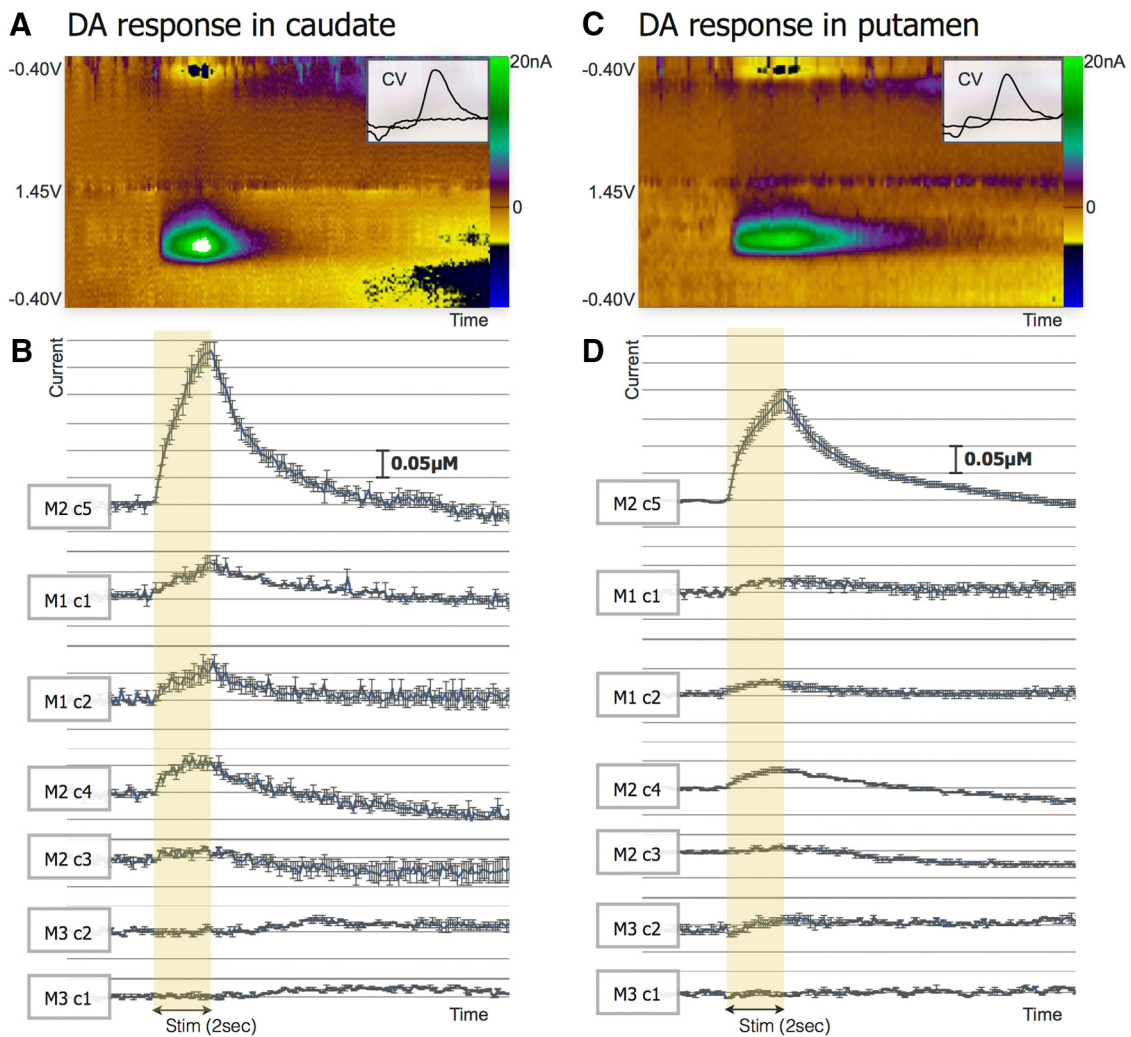


Figure 2. DBS-evoked dopamine (DA) response. **A**, Representative pseudocolor plot of STN stimulation-evoked change in caudate DA as analyzed by voltammetry. **B**, Mean \pm SEM DA oxidation current versus time plot of stimulation-evoked DA release in the caudate relative to a single subject and a single contact as marked in the left panel (average of $n = 3$ data points). **C**, Representative pseudocolor plot of STN stimulation-evoked change in DA putamen as measured by voltammetry. **D**, Mean \pm SEM DA oxidation current versus time plot of stimulation-evoked DA release in the putamen relative to a single subject and a single contact as marked in the left panel (average of $n = 3$ data points).

throughout motor and nonmotor circuitry (Min et al., 2014). Figure 1*H,J* shows a representative single subject (M1) and single-scan fMRI of STN DBS-evoked BOLD activation in the caudate and the putamen, respectively. Figure 1*I,K* depicts the STN stimulation-induced dopamine response to the targeted sites in the caudate and putamen, respectively. In all three subjects, the dopamine response was maximal at the individual maximum t -score BOLD voxel with an error of 1.85 ± 0.37 mm. Dopamine was measured continuously in at a depth of 0.42 ± 0.04 mm.

Dopamine release in the caudate and the putamen

Figure 2 shows pseudocolor plots of dopamine oxidation and reduction, the temporal pattern of stimulation time-locked caudate and putamen dopamine release across the three subjects, and 3-D models of DBS contact locations in the STN. As shown in Figure 2*A,C* (right panel insets), the recorded cyclic voltammograms exhibited an oxidation peak at $+0.6$ V and a reduction peak at -0.2 V, which is consistent with the oxidation and reduction of dopamine. Of the 17 DBS contacts in the STN across the three subjects, 10 contacts evoked dopamine release in the caudate and nine evoked dopamine release in the putamen. Figure 2*B,D* shows the mean \pm SEM ($n = 3$) dopamine oxidation current versus time plots of STN stimulation-

evoked dopamine release in the caudate and putamen from seven representative DBS contacts.

We overlaid an evoked dopamine response volume projection color map from the caudate (Fig. 3*A–C*) and the putamen (Fig. 3*D–F*) onto the 3-D STN DBS contact location model. The evoked dopamine response color map shows increased dopamine release when stimulating an area adjacent to the posterior and lateral border of the STN. The dopamine responses in the caudate and the putamen were similar to one another in that the concentration of dopamine increased when stimulating posterior and lateral portions of the STN and maximized when the location of stimulation was just beyond the dorsolateral posterior border of the STN (Fig. 3*A,D*, coronal view; Fig. 3*B,E*, sagittal view; Fig. 3*C,F*, axial view; per neurological convention). However, the average amount of evoked dopamine from the seven representative contacts in the putamen was $51 \pm 4\%$ (mean \pm SEM) less than that from the caudate (Fig. 2*B,D*).

Relationship between STN stimulation site and caudate/putamen dopamine release

We conducted Pearson correlation analysis to determine the significance of the relationship between the peak magnitude of the

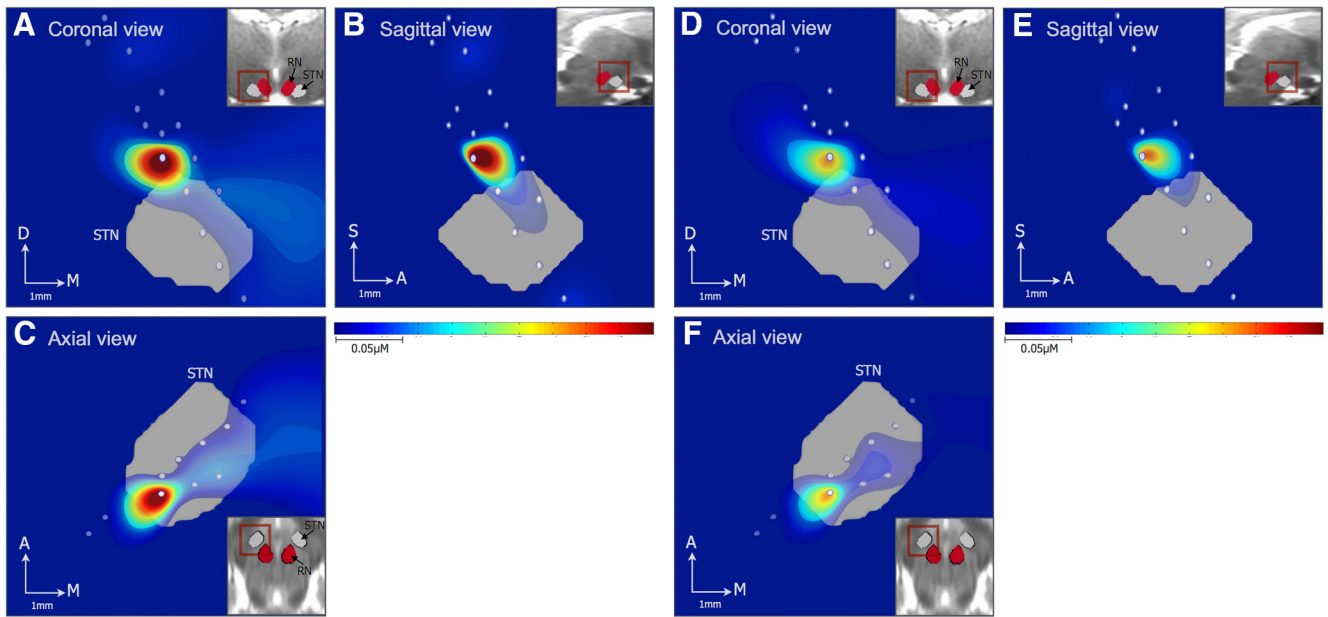


Figure 3. STN DBS stimulation site-dependent dopamine (DA) response projection map. **A–F**, To show the volume of DA released in caudate and putamen evoked by each stimulation contact, we overlaid an evoked-DA response volume projection color map (bilinear interpolation) from the caudate (**A–C**) and the putamen (**D–F**) onto the 3-D STN DBS contact location model in views representing neurologic convention. Coronal view (**A**), sagittal view (**B**), and axial view (**C**) of STN stimulation-dependent differences in caudate DA release ($n = 51$, stimulation sessions). Coronal view (**D**), sagittal view (**E**), and axial view (**F**) of STN stimulation-dependent differences in putamen DA release ($n = 51$, stimulation sessions). DA release in both caudate and putamen was increased when the location of stimulation was just outside the dorsolateral posterior border of the STN, a location that would contain the nigrostriatal fibers that run just dorsal to the STN.

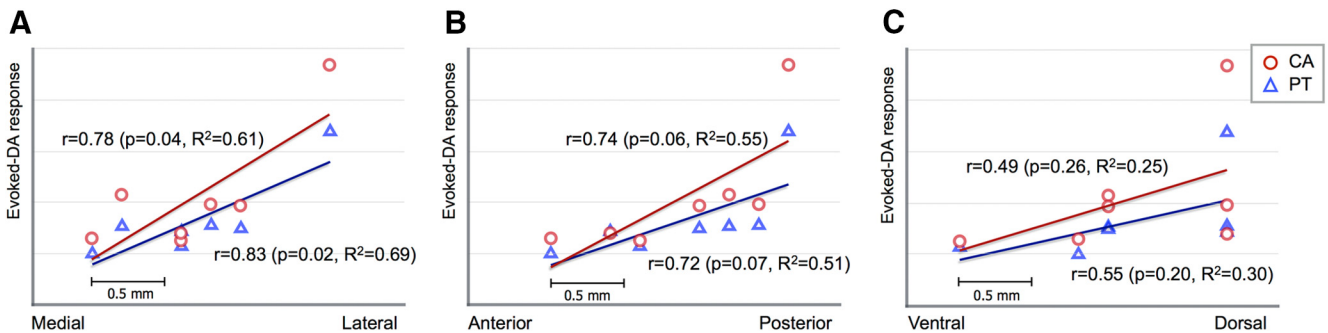


Figure 4. Directional relationship of STN stimulation site with evoked dopamine (DA) release in the caudate (CA; circles) and putamen (PT; triangles). **A**, Relationship between electrode position in the STN (medial to lateral) and evoked DA release in the CA and in the PT. **B**, Relationship between electrode position in the STN (anterior to posterior) evoked DA release in the CA and the PT. **C**, Relationship between electrode position (ventral to dorsal) and evoked DA release in the CA and the PT.

evoked dopamine response in the caudate and putamen and the position of the seven contacts in the dorsal part of STN that evoked dopamine relative to Cartesian coordinates (origin at anterior commissure aligned with posterior commissure). There was a significant correlation between stimulation in the medial-to-lateral axis of the STN and dopamine release in the caudate ($r = 0.78$; $p = 0.04$) and in the putamen ($r = 0.83$; $p = 0.02$; Fig. 4A). Similarly, there was a trend toward a significant relationship between stimulation in the anterior-to-posterior plane of the STN and dopamine release in the caudate ($r = 0.74$; $p = 0.06$) and in the putamen ($r = 0.72$; $p = 0.07$; Fig. 4B). There were no significant relationships between stimulation in the ventral-dorsal plane and dopamine release in either the caudate ($r = 0.49$; $p = 0.26$) or the putamen ($r = 0.55$; $p = 0.20$; Fig. 4C).

Discussion

In an effort to reconcile differences among clinical and preclinical studies of STN DBS-evoked dopamine release, we investigated the relationship between stimulation site in the STN and DBS-

evoked dopamine release in the caudate and putamen. We found a spatial distribution in which the magnitude of DBS-evoked dopamine release increased when the stimulation was delivered to a more lateral and posterior site. Specifically, dopamine release peaked in the fMRI targeted sites in both the caudate and putamen when stimulating the dorsolateral posterior border of the STN. Although these tests involved an intact brain, these findings suggest that STN DBS evokes dopamine release and that its concentration varies depending on the site being stimulated.

Several nonexclusionary explanations have been proposed to support the potential effects of STN stimulation on midbrain dopaminergic neuronal activity. It is known that a proportion of STN excitatory glutamatergic neurons projects to dopaminergic dendrites and inhibitory interneuronal GABAergic cells in the substantia nigra pars reticulata (SNr; Kita and Kitai, 1987). If DBS partially inhibits STN outflow via depolarization blockade, it would lead to reduced excitation of SNr GABAergic neurons (Benazzouz et al., 2000), which themselves inhibit substantia

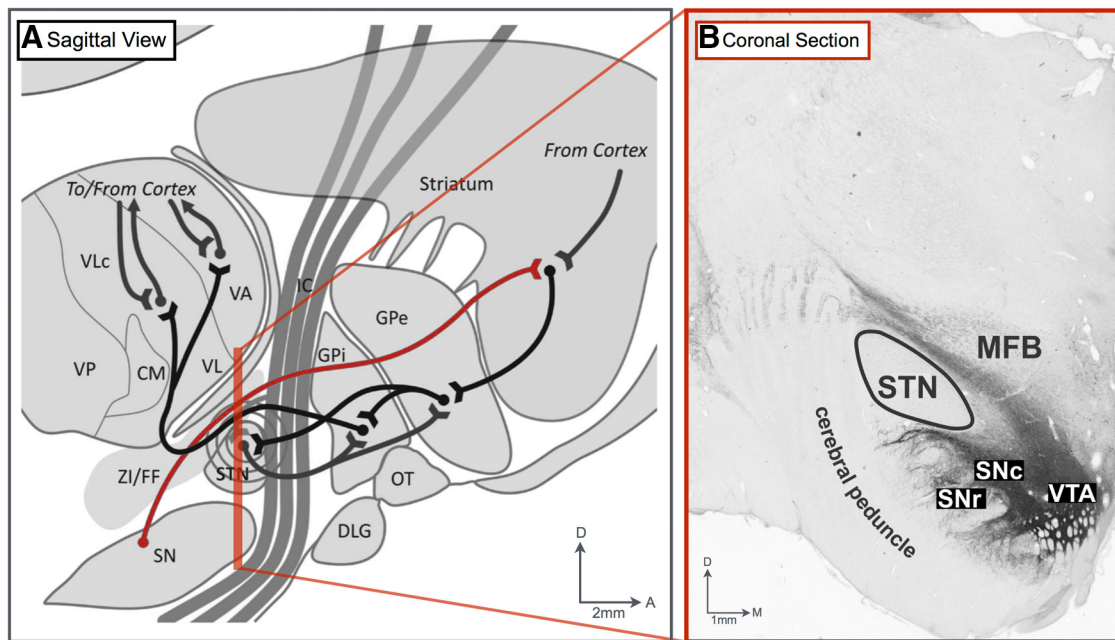


Figure 5. Major anatomical pathways affected by STN stimulation. **A**, Diagram of the sagittal view of the location of the STN in relation to the medial forebrain bundle (red line) comprising the ascending dopaminergic nigrostriatal and mesocorticolimbic pathways. Diagram reprinted with permission from Devergnas and Wichmann, 2011. **B**, Representative coronal section of tyrosine hydroxylase immunohistochemical analysis of dopaminergic projections in relation to the STN (Gale et al., 2013). VTA, Ventral tegmental area.

nigra compacta (SNc) dopaminergic neurons (Grace and Bunney, 1979) and thereby indirectly increase dopamine neuronal firing (disinhibition; Meissner et al., 2003). In addition, electrical stimulation may also increase the activity of a population of glutamatergic STN neuronal projections to SNc dopaminergic neurons, thereby directly increasing their activity (Chergui et al., 1994; Windels et al., 2000).

An additional possibility is that electrical stimulation activates SNc efferent nigrostriatal fibers in close proximity to the STN, as observed in rodent studies of medial forebrain bundle stimulation (Lee et al., 2006). As shown in Figure 5A,B, midbrain-originating nigrostriatal and mesocorticolimbic dopamine-containing fibers ascend to forebrain structures along a ventral-to-dorsal aspect of the STN in NHPs (Devergnas and Wichmann, 2011), a pathway considered analogous to that in humans (Parent et al., 2000). When seen in a sagittal view, this ventrodorsal dopaminergic projection also appears very close to the posterior aspect of the STN (Fig. 5A). Our results, also suggest that these white matter areas are close enough to the STN to be affected by stimulation of the dorsolateral posterior STN contacts.

Two factors that might have influenced our findings of DBS-evoked changes in dopamine release in the caudate and putamen are (1) variability in the location of the dopamine recording site and (2) variability in the location of the stimulating electrode within the STN. To reduce variability in the dopamine recording site across subjects, we identified an optimal recording site using fMRI as a guide for positioning the sensing tip of the recording electrode in each subject. The dopamine response across the three subjects was obtained only when the sensing tip was within the fMRI-identified recording site in the caudate and putamen. The fact that there was a similar pattern of dopamine distribution in the caudate and the putamen of all three subjects supports the possibility that our results are related to something other than individual variability in the neurochemical recording site.

To address the second factor, potential differences in dopamine release relative to the stimulation site in the STN, it was

necessary to ensure accuracy of targeting and precise electrode location by more than one method. We increased the resolution and contrast while maintaining minimum geometric distortion of the MRI during DBS surgical targeting and were able to reach submillimeter accuracy in phantom tests (Min et al., 2014). The electrode location was also confirmed postoperatively by imaging and histology.

When investigating differences in the effects of individual stimulation contacts, the size of the current diffusion from the electrode must be taken into account (Mallet et al., 2007). A large current diffusion effect can overwhelm small differences in contact location. The miniature electrodes in this study exhibit a current density of $\sim 20 \mu\text{C}/\text{cm}^2$, which is comparable in order of magnitude to the $\sim 10 \mu\text{C}/\text{cm}^2$ of human DBS electrodes. Our results argue for a current distribution effect on the order of <1 mm, which has been previously reported and discussed relative to human DBS electrodes (McIntyre et al., 2004; Mallet et al., 2007). The slightly higher current density effect of our miniature DBS electrodes may have caused a steeper current drop relative to distance from individual contacts (Lozano et al., 2002), which in turn could have resulted in more distinct differences among contacts. However, this effect was likely compensated for by the proportional difference in brain size between the human and the NHP and the scaled-down dimensions of the DBS electrodes used.

It is of note that STN DBS-evoked motor symptom improvement in patients with PD has been found to be optimal when the DBS electrode projects onto white matter dorsal to the STN (Saint-Cyr et al., 2002), including the dorsolateral border of the STN (Starr et al., 2002; Herzog et al., 2004). These clinical reports and the present findings of an STN DBS dopamine effect are at odds with the failure to find a similar effect in the previously mentioned RAC PET studies of PD patients whose motor symptoms were reduced by DBS. A factor that may account for these differences is the use in our study of subjects with intact brains, rather than subjects with PD. Given that degenerated dopaminergic

gic cells are a major factor in PD pathology, the magnitude of stimulation-evoked dopamine release observed in our subjects might have been muted in the RAC PET studies of subjects with PD. In addition, *in vivo* electrochemical techniques provide localized and direct monitoring of evoked dopamine release (Garris et al., 1994). PET, on the other hand, relies on an indirect, model-based global tissue assessment (Brooks, 2001) that impedes the detection of small, site-specific changes in striatal dopamine levels. That said, because DBS is usually reserved for late-stage PD, when dopamine agonists have either reduced effectiveness or cause intolerable levels of adverse effects (dyskinesias), it will be important to test our findings in large animal models of PD and eventually in patients with PD who are undergoing DBS and in whom dopamine function is significantly reduced.

The timing and duration of stimulation in the RAC PET studies and preclinical studies differs as well. Dopamine turnover time in within-subject rodent studies requires short-term stimulation with a minimum of several minutes between stimulation to account for reuptake and repackaging in the presynaptic area (Garris et al., 1994). Such was also the case in our study.

Last, it should be noted that there was individual variability in dopamine levels among the subjects in the RAC PET studies. While the group average showed no significant differences, several subjects did show RAC displacement in the DBS ON condition (Abosch et al., 2003; Hilker et al., 2003), which, given our results, suggests that the precise location of the stimulation contact may affect group results.

Our findings regarding the dependence of dopamine release relative to the STN stimulation site may also have implications for the adverse effects that can occur in STN DBS for PD. Hypomania and impulsivity are known to occur with STN DBS for PD (Chopra et al., 2011) and can also occur with poorly regulated dopaminergic medications in PD (Beaulieu-Boire and Lang, 2015). Specifically, it has been reported that while dorsal STN DBS improves motor function, ventral STN stimulation can be associated with hypomania (Mallet et al., 2007). During STN DBS surgical targeting, the electrode trajectory is positioned at an angle from the anterior dorsal border of the prefrontal cortex to a posterior ventral passage through the horizontal line of the anterior border of the RN (as seen in the axial view, which displays the RN most prominently; Starr et al., 2002). As a result, in clinical DBS, the ventral STN contact is typically placed in the posterior aspect of the STN relative to the dorsal contacts. The medial forebrain bundle consists of axons of the dopaminergic nigrostriatal, mesocorticolimbic, and other neurotransmitter systems (Fig. 5A).

This study demonstrates that in the intact NHP, dopamine release can be reduced or increased by subtle changes in the STN stimulation site. If supported by further studies, these findings of site-specific STN DBS-evoked dopamine release could have implications for understanding the circuitry effects of STN DBS, since stimulated brain networks are anatomically and functionally segregated within the basal ganglia thalamocortical system and are represented in distinct functional motor, associative, and limbic cortical regions (DeLong and Wichmann, 2012). Further studies investigating the effects of stimulation site-dependent DBS-evoked dopamine release in PD animal models and on positive behavioral outcomes and adverse effects of STN DBS are needed to substantiate these initial findings.

References

- Abosch A, Kapur S, Lang AE, Hussey D, Sime E, Miyasaki J, Houle S, Lozano AM (2003) Stimulation of the subthalamic nucleus in Parkinson's disease does not produce striatal dopamine release. *Neurosurgery* 53:1095–1102, discussion 1102–1105. [CrossRef Medline](#)
- Beaulieu-Boire I, Lang AE (2015) Behavioral effects of levodopa. *Mov Disord* 30:90–102. [CrossRef Medline](#)
- Benabid AL, Benazzouz A, Limousin P, Koudsie A, Krack P, Piallat B, Pollak P (2000) Dyskinesias and the subthalamic nucleus. *Ann Neurol* 47:S189–S192. [Medline](#)
- Benazzouz A, Gao DM, Ni ZG, Piallat B, Bouali-Benazzouz R, Benabid AL (2000) Effect of high-frequency stimulation of the subthalamic nucleus on the neuronal activities of the substantia nigra pars reticulata and ventrolateral nucleus of the thalamus in the rat. *Neuroscience* 99:289–295. [CrossRef Medline](#)
- Brooks DJ (2001) Functional imaging studies on dopamine and motor control. *J Neural Transm (Vienna)* 108:1283–1298. [CrossRef Medline](#)
- Bruet N, Windels F, Bertrand A, Feuerstein C, Poupard A, Savasta M (2001) High frequency stimulation of the subthalamic nucleus increases the extracellular contents of striatal dopamine in normal and partially dopaminergic denervated rats. *J Neuropathol Exp Neurol* 60:15–24. [CrossRef Medline](#)
- Chang SY, Kim I, Marsh MP, Jang DP, Hwang SC, Van Gompel JJ, Goerss SJ, Kimble CJ, Bennet KE, Garris PA, Blaha CD, Lee KH (2012) Wireless fast-scan cyclic voltammetry to monitor adenosine in patients with essential tremor during deep brain stimulation. *Mayo Clin Proc* 87:760–765. [CrossRef Medline](#)
- Chang SY, Kimble CJ, Kim I, Paek SB, Kressin KR, Boesche JB, Whitlock SV, Eaker DR, Kasasbeh A, Horne AE, Blaha CD, Bennet KE, Lee KH (2013) Development of the Mayo Investigational Neuromodulation Control System: toward a closed-loop electrochemical feedback system for deep brain stimulation. *J Neurosurg* 119:1556–1565. [CrossRef Medline](#)
- Chergui K, Akaoka H, Charl y P, Saunier CF, Buda M, Chouvet G (1994) Subthalamic nucleus modulates burst firing of nigral dopamine neurones via NMDA receptors. *Neuroreport* 5:1185–1188. [CrossRef Medline](#)
- Chopra A, Tye SJ, Lee KH, Matsumoto J, Klassen B, Adams AC, Stead M, Sampson S, Kall BA, Frye MA (2011) Voltage-dependent mania after subthalamic nucleus deep brain stimulation in Parkinson's disease: a case report. *Biol Psychiatry* 70:e5–e7. [CrossRef Medline](#)
- DeLong M, Wichmann T (2012) Deep brain stimulation for movement and other neurologic disorders. *Ann NY Acad Sci* 1265:1–8. [CrossRef Medline](#)
- Devergnas A, Wichmann T (2011) Cortical potentials evoked by deep brain stimulation in the subthalamic area. *Front Sys Neurosci* 5:30. [CrossRef Medline](#)
- Gale JT, Lee KH, Amirnovin R, Roberts DW, Williams ZM, Blaha CD, Eskandar EN (2013) Electrical stimulation-evoked dopamine release in the primate striatum. *Stereotact Funct Neurosurg* 91:355–363. [CrossRef Medline](#)
- Garris PA, Ciolkowski EL, Pastore P, Wightman RM (1994) Efflux of dopamine from the synaptic cleft in the nucleus accumbens of the rat brain. *J Neurosci* 14:6084–6093. [Medline](#)
- Grace AA, Bunney BS (1979) Paradoxical GABA excitation of nigral dopaminergic cells: indirect mediation through reticulata inhibitory neurons. *Eur J Pharmacol* 59:211–218. [CrossRef Medline](#)
- Heien ML, Phillips PE, Stuber GD, Seipel AT, Wightman RM (2003) Over-oxidation of carbon-fiber microelectrodes enhances dopamine adsorption and increases sensitivity. *Analyst* 128:1413–1419. [CrossRef Medline](#)
- Herzog J, Fietzek U, Hamel W, Morsnowski A, Steigerwald F, Schrader B, Weiert D, Pfister G, M ller D, Mehdorn HM, Deuschl G, Volkmann J (2004) Most effective stimulation site in subthalamic deep brain stimulation for Parkinson's disease. *Mov Disord* 19:1050–1054. [CrossRef Medline](#)
- Hilker R, Voges J, Ghaemi M, Lehrke R, Rudolf J, Koulousakis A, Herholz K, Wienhard K, Sturm V, Heiss WD (2003) Deep brain stimulation of the subthalamic nucleus does not increase the striatal dopamine concentration in parkinsonian humans. *Mov Disord* 18:41–48. [CrossRef Medline](#)
- Kita H, Kitai ST (1987) Efferent projections of the subthalamic nucleus in the rat: light and electron microscopic analysis with the PHA-L method. *J Comp Neurol* 260:435–452. [CrossRef Medline](#)
- Kringelbach ML, Jenkinson N, Owen SL, Aziz TZ (2007) Translational principles of deep brain stimulation. *Nat Rev Neurosci* 8:623–635. [CrossRef Medline](#)

- Lauro PM, Vanegas-Arroyave N, Huang L, Taylor PA, Zaghoul KA, Lungu C, Saad ZS, Horovitz SG (2016) DBSproc: an open source process for DBS electrode localization and tractographic analysis. *Hum Brain Mapp* 37:422–433. [CrossRef Medline](#)
- Lee KH, Blaha CD, Harris BT, Cooper S, Hitti FL, Leiter JC, Roberts DW, Kim U (2006) Dopamine efflux in the rat striatum evoked by electrical stimulation of the subthalamic nucleus: potential mechanism of action in Parkinson's disease. *Eur J Neurosci* 23:1005–1014. [CrossRef Medline](#)
- Lozano AM, Dostrovsky J, Chen R, Ashby P (2002) Deep brain stimulation for Parkinson's disease: disrupting the disruption. *Lancet Neurol* 1:225–231. [CrossRef Medline](#)
- Mallet L, Schüpbach M, N'Diaye K, Remy P, Bardinet E, Czernecki V, Welter ML, Pelissolo A, Ruberg M, Agid Y, Yelnik J (2007) Stimulation of subterritories of the subthalamic nucleus reveals its role in the integration of the emotional and motor aspects of behavior. *Proc Natl Acad Sci U S A* 104:10661–10666. [CrossRef Medline](#)
- McIntyre CC, Mori S, Sherman DL, Thakor NV, Vitek JL (2004) Electric field and stimulating influence generated by deep brain stimulation of the subthalamic nucleus. *Clin Neurophysiol* 115:589–595. [CrossRef Medline](#)
- Meissner W, Harnack D, Reese R, Paul G, Reum T, Ansorge M, Kusserow H, Winter C, Morgenstern R, Kupsch A (2003) High-frequency stimulation of the subthalamic nucleus enhances striatal dopamine release and metabolism in rats. *J Neurochem* 85:601–609. [CrossRef Medline](#)
- Min HK, Ross EK, Lee KH, Dennis K, Han SR, Jeong JH, Marsh MP, Striemer B, Felmlee JP, Lujan JL, Goerss S, Duffy PS, Blaha CD, Chang SY, Bennet KE (2014) Subthalamic nucleus deep brain stimulation induces motor network BOLD activation: use of a high precision MRI guided stereotactic system for nonhuman primates. *Brain Stimul* 7:603–607. [CrossRef Medline](#)
- Moro E, Scerrati M, Romito LM, Roselli R, Tonali P, Albanese A (1999) Chronic subthalamic nucleus stimulation reduces medication requirements in Parkinson's disease. *Neurology* 53:85–90. [CrossRef Medline](#)
- Parent A, Cossette M, Levesque M (2000) Anatomical considerations in basal ganglia surgery. In: *Movement Disorders* (Lozano AM, ed), pp 21–30. Basel: Karger.
- Saint-Cyr JA, Hoque T, Pereira LC, Dostrovsky JO, Hutchison WD, Mikulis DJ, Abosch A, Sime E, Lang AE, Lozano AM (2002) Localization of clinically effective stimulating electrodes in the human subthalamic nucleus on magnetic resonance imaging. *J Neurosurg* 97:1152–1166. [CrossRef Medline](#)
- Shen H (2014) Neuroscience: tuning the brain. *Nature* 507:290–292. [CrossRef Medline](#)
- Shon YM, Lee KH, Goerss SJ, Kim IY, Kimble C, Van Gompel JJ, Bennet K, Blaha CD, Chang SY (2010) High frequency stimulation of the subthalamic nucleus evokes striatal dopamine release in a large animal model of human DBS neurosurgery. *Neurosci Lett* 475:136–140. [CrossRef Medline](#)
- Starr PA, Christine CW, Theodosopoulos PV, Lindsey N, Byrd D, Mosley A, Marks WJ Jr (2002) Implantation of deep brain stimulators into the subthalamic nucleus: technical approach and magnetic resonance imaging-verified lead locations. *J Neurosurg* 97:370–387. [CrossRef Medline](#)
- Strafella AP, Sadikot AF, Dagher A (2003) Subthalamic deep brain stimulation does not induce striatal dopamine release in Parkinson's disease. *Neuroreport* 14:1287–1289. [CrossRef Medline](#)
- Szeliski R (1990) Fast surface interpolation using hierarchical basis functions. *IEEE T Pattern Anal* 12:513–528. [CrossRef](#)
- Thobois S, Fraix V, Savasta M, Costes N, Pollak P, Mertens P, Koudsie A, Le Bars D, Benabid AL, Broussolle E (2003) Chronic subthalamic nucleus stimulation and striatal D2 dopamine receptors in Parkinson's disease—a [(11)C]-raclopride PET study. *J Neurol* 250:1219–1223. [CrossRef Medline](#)
- Van Essen DC, Glasser MF, Dierker DL, Harwell J (2012) Cortical parcellations of the macaque monkey analyzed on surface-based atlases. *Cereb Cortex* 22:2227–2240. [CrossRef Medline](#)
- Windels F, Bruet N, Poupard A, Urbain N, Chouvet G, Feuerstein C, Savasta M (2000) Effects of high-frequency stimulation of subthalamic nucleus on extracellular glutamate and GABA in substantia nigra and globus pallidus in the normal rat. *Eur J Neurosci* 12:4141–4146. [CrossRef Medline](#)
- Yushkevich PA, Piven J, Hazlett HC, Smith RG, Ho S, Gee JC, Gerig G (2006) User-guided 3D active contour segmentation of anatomical structures: significantly improved efficiency and reliability. *Neuroimage* 31:1116–1128. [CrossRef Medline](#)